IEEE Access
Multidisciplinary | Rapid Review | Open Access Journal

Received July 22, 2019, accepted August 19, 2019, date of publication August 26, 2019, date of current version September 11, 2019.

Digital Object Identifier 10.1109/ACCESS.2019.2937571

Knock Detection Based on Recursive Variational Mode Decomposition and Multilevel Semi-Supervised Local Fisher Discriminant Analysis

FENGRONG BI, XIN LI, JIEWEI LIN, XIAOBO BI, TENG MA, XIAO YANG, DAIJIE TANG, AND PENGFEI SHEN

State Key Laboratory of Engines, Tianjin University, Tianjin 300072, China

Corresponding author: Jiewei Lin (linjiewei@tju.edu.cn)

This work was supported by the National Natural Science Foundation of China under Project 51705357.

ABSTRACT Knock is an abnormal combustion phenomenon in gasoline engines. Strong knocks will reduce the efficiency and durability of engine, while with slight knocks engines can run on a high-efficiency state. It is necessary to detect knock and control the state of knock in order to improve the thermal efficiency of engine. This paper proposes a novel approach for detecting engine knocks in various intensities based on vibration signal of engine block using variational mode decomposition (VMD) and semi-supervised local fisher discriminant analysis (SELF). Since the quadratic penalty of recursive VMD has a great influence on decomposition results, the approach establishes the connection between the quadratic penalty and the stop condition by analyzing a large amount of data and quantifies the relationship by polynomial fitting, which reduces the complexity and subjectivity of recursive VMD. A multilevel SELF is developed for solving the problem that SELFs sometimes may not find ideal embedding space under large scale dimensionality reduction. This method adopts multi embedding spaces, with gradually decreasing dimension, to reduce the dimensionality of original data by a series of small steps. Verifications show the proposed approach can achieve high classification accuracy in knock detection and is able to identify the intensity of knock. This research contributes to the field of engine abnormality detection and can be implemented on vibration-based faults diagnosis area.

INDEX TERMS Engine, knock detection, semi-supervised local fisher discriminant analysis (SELF), variational mode decomposition (VMD), vibration.

I. INTRODUCTION

As a major power source, engines are being widely used in industry, agriculture and transportation, and playing an important role in economy and daily life. Under global energy and environmental crisis, the economy and emission of engines have become hot issues. For this reason, down-sizing and strengthening techniques, represented by turbo charge and direct-injection, become one of the main research directions for engine [1]. However, the following problem of knock seriously hindered the development of gasoline engine. Knock is an abnormal combustion phenomenon. Strong knocks will reduce the efficiency and durability of engine, while slight knocks can make it run in approximately constant volume combustion state so as to increase efficiency greatly [2]. So, detecting knock to keep engine operating with slight knock has great value in theoretical research and engineering application.

In knock detection, cylinder pressure [3], combustion noise [4] and engine block vibration [5] are widely used. The cylinder pressure detection method needs expensive sensors and is usually applied in research. The combustion noise detection method can be easily interfered by external factors. The engine block vibration detection is the most popular method in engineering application because of its low cost and simplicity.

There is lots of noise in engine block vibration signals, which has little influence on strong knock characteristics

The associate editor coordinating the review of this article and approving it for publication was Lorenzo Mucchi.

but is easy to cover up slight knocks. Many efforts have been made on signal processing, including traditional time-frequency analysis, wavelet analysis, empirical mode decomposition (EMD) and so on [6]–[8]. Sharma *et al.* [9] used short time Fourier transform (STFT) to analyze engine vibration signals and obtained the characteristics of abnormal combustion. Taghizadeh-Alisaraei *et al.* [10] found 3D Morlet wavelet scalogram can provide higher resolution in analyzing engine knock. Yadav *et al.* [11] combined the intrinsic mode functions (IMFs) decomposed by EMD with fault features and achieved more accurate results. However, traditional time-frequency analysis method, such as STFT, cannot reach a high enough resolution both in time and frequency domains. Besides, the wavelet analysis is not a self-adaptation decomposition method either [12]. EMD is a self-adaptation method, but its native defects, such as mode mixing and struggling in decomposing IMFs with close frequencies, brought by recursive model still puzzle researchers [13], [14]. Although ensemble empirical mode decomposition (EEMD) can solve the mode mixing to certain extent, it is accompanied by influences of low efficiency and residual white noise [15], [16]. To overcome these problems, Dragomiretskiy and Zosso [17] proposed variational mode decomposition (VMD) based on variational principle. Essentially the VMD is multilevel Wiener filtering which has higher accuracy and efficiency because of abandoning recursive model, and has shown great potential in faults detection [18], [19]. However, several control parameters in VMD, such as decomposition level K and quadratic penalty α, have to be determined manually, which brings subjective effect and reduces the accuracy and efficiency of VMD.

After signals decomposition, characteristic parameters should be extracted to recognize working conditions. Lots of characteristic parameters are able to describe signals in different aspects. In this case, too few characteristic parameters cannot describe the features clearly, while too many will increase the complexity of classifier without increase in accuracy [20]. To solve this problem, dimensionality reduction method was introduced to process characteristic parameters to improve the generalization and efficiency of classifier [21]. Principal component analysis (PCA) and local Fisher discriminant analysis (LFDA) are the two representative methods widely used in many fields [22], [23]. The LFDA, a supervised dimensionality reduction method, cannot ensure a high accuracy if the labeled samples are inappropriate. On the contrary, the PCA is an unsupervised dimensionality reduction, which is not necessary to get the best results for the samples with great scaling difference. In 2010, Sugiyama *et al.* [24] proposed semi-supervised local Fisher discriminant analysis (SELF), which could connect PCA and LFDA smoothly to mitigate their defects. SELF shows great performance in application, such as face recognition [25], speech recognition [26], gene expression data recognition [27] and so on. However, the application of SELF in engine vibration signals is immature and needs further adaptive optimization.

To solve the problems mentioned above, this paper proposes a novel approach for detecting knocks in different intensities based on engine block vibration. The paper is organized as follows: Section 1 introduces research background and significance, Section 2 gives algorithms details, the experiment is described in Section 3, recursive VMD is optimized in Section 4, multilevel SELF is proposed in Section 5, and conclusion and discussion are given in Section 6.

II. ALGORITHM THEORIES

VMD and SELF are the core algorithms for this work and their basic theories are introduced in this section.

A. VMD ALGORITHM THEORIES

The purpose of VMD is to decompose an input signal f into several IMFs u_k. Every u_k compacts around a center frequency ω_k, which is determined by decomposition level. Each u_k has a specific sparsity and all of them could restructure the input signal f [17].

Firstly, u_k should be processed by Hilbert transformation to get its unilateral spectrum:

$$H = \left[\delta(\mathrm{t}) + \frac{\mathrm{j}}{\pi t}\right] u_k(t) \tag{1}$$

where δ represents Fermi-Dirac distribution, $\mathrm{j}^2 = -1$, $k \in \{1, 2, \cdots, K\}$ and K is the decomposition level.

Secondly, an estimated center frequency, $\mathrm{e}^{-\mathrm{j}\omega_k t}$, is blended into the unilateral spectrum of u_k and the frequency domain of u_k will be transformed into baseband:

$$B = \left[\delta(\mathrm{t}) + \frac{\mathrm{j}}{\pi t}\right] u_k(t) * \mathrm{e}^{-\mathrm{j}\omega_k t} \tag{2}$$

where $*$ represents convolutions.

Then, the bandwidth of u_k could be obtained by H^1 Gauss smoothing, i.e. L^2 norm:

$$\begin{aligned} &\min_{\{u_k\},\{w_k\}} \left\{ \sum_k \left\| \partial_{\mathrm{t}} \left[\delta(\mathrm{t}) + \frac{\mathrm{j}}{\pi t}\right] u_k(t) * \mathrm{e}^{-\mathrm{j}\omega_k t} \right\|_2^2 \right\}, \\ &s.t \qquad \sum_k u_k = f \end{aligned} \tag{3}$$

where $\{u_k\} := \{u_1, u_2, \cdots, u_k\}$ and $\{\omega_k\} := \{\omega_1, \omega_2, \cdots, \omega_{\mathrm{k}}\}$ are shorthands of IMFs and their center frequencies, respectively. $\sum_k := \sum_{k=1}^{K}$ is the summation of all IMFs.

Equation (3) is a constrained variational model and can be transformed into an unconstrained variational model by introducing quadratic penalty α and Lagrange multiplier λ. So the augmented Lagrange formula is:

$$\begin{aligned} &L(\{u_k\}, \{\omega_k\}, \lambda) : \\ &= \alpha \sum_k \left\| \partial_t [(\delta(t) + \frac{\mathrm{j}}{\pi t}) * u_k(t)] e^{-\mathrm{j}\omega_k t} \right\|_2^2 \\ &\quad + \left\| f(t) - \sum_k u_k(t) \right\|_2^2 + \left\langle \lambda(t), f(t) - \sum_k u_k(t) \right\rangle \end{aligned} \tag{4}$$

This is a classic method to solve constrained variational model. The α has a great influence on decomposing results and the selection of it will be researched in following contents.

This is a Lagrange saddle point problem and the results are:

$$\widehat{u}_k^{n+1}(\omega) = \frac{\widehat{f}(\omega) - \sum_{i\neq k}\widehat{u}_i(\omega) + \frac{\widehat{\lambda}(\omega)}{2}}{1 + 2\alpha(\omega - \omega_k)^2} \tag{5}$$

$$\omega_k^{n+1} = \frac{\int_0^\infty \omega \left|\widehat{u}_k(\omega)\right|^2 d\omega}{\int_0^\infty \left|\widehat{u}_k(\omega)\right|^2 d\omega} \tag{6}$$

$$\widehat{\lambda}^{n+1}(\omega) = \widehat{\lambda}^n(\omega) + \tau(\widehat{f}(\omega) - \sum_k u_k^{n+1}) \tag{7}$$

where τ represents the update parameter.

According to (5), (6) and (7), final results can be obtained by alternate direction method of multipliers (ADMM). At this point, the detailed workflow of VMD can be given as:

① Initialize $\left\{\widehat{u}_k^1\right\}$, $\left\{\omega_k^1\right\}$, and $\widehat{\lambda}^1$, and set the number of cycles $n = 1$.

② Update u_k by (5).

③ Update ω_k by (6).

④ Update λ by (7).

⑤ Set $n = n + 1$, and repeat the steps ② -④.

⑥ Output results when cut-off condition is met. The cut-off condition of VMD is:

$$\sum_k \left\|\widehat{u}_k^{n+1} - \widehat{u}_k^n\right\|_2^2 / \left\|\widehat{u}_k^n\right\|_2^2 < \varepsilon \tag{8}$$

In general, $\varepsilon = 10^{-7}$.

As soon as the iteration is completed, K IMFs can be obtained.

B. SELF ALGORITHM THEORIES

SELF is an algorithm for dimensionality reduction, whose purpose is to obtain low-dimensional representation of high-dimensional data as well as retain most inner information of original data [24].

Suppose $x_i \in R^d (i = 1, 2, \cdots n)$ is a d-dimensional vector and $X \in R^{d\times n}$ is the matrix composed of x_i:

$$X := (x_1 | x_2 | \cdots | x_n) \tag{9}$$

Let $z \in R^r (1 \leq r \leq d)$ be the low-dimensional representation of the high-dimensional sample $x \in R^d$, where r is the dimensionality of reduced space. This can be realized by transformation matrix $T \in R^{d\times r}$:

$$z = T^{\mathrm{T}}x \tag{10}$$

where the superscript T represents the transpose of a matrix or a vector.

The dimensionality reduction is to solve the transformation matrix $T \in R^{d\times r}$. Its general form is:

$$T^{(OPT)} := \arg\max_{T\in R^{d\times r}}[\mathrm{tr}(T^{\mathrm{T}}BT(T^{\mathrm{T}}CT)^{-1})] \tag{11}$$

where $T^{(OPT)}$: represents the optimal transformation matrix. B is the matrix composed of values that need increasing, e.g. between-class separability. C is the matrix composed of values that need reducing, e.g. within-class separability.

Since SELF is a combination of PCA and LFDA, basics of the two algorithms are given as follows:

1) PCA ALGORITHM

Suppose $S^{(t)}$ is total scatter matrix:

$$S^{(t)} := \sum_{i=1}^n (x_i - \mu)(x_i - \mu)^{\mathrm{T}} \tag{12}$$

where μ is the mean of samples: $\mu = \frac{1}{n}\sum_{i=1}^n x_i$.

The transformation matrix in PCA, $T^{(\mathrm{PCA})}$, is:

$$T^{(\mathrm{PCA})} := \arg\max_{T\in R^{d\times r}}[\mathrm{tr}(T^{\mathrm{T}}S^{(t)}T(T^{\mathrm{T}}T)^{-1})] \tag{13}$$

Compared with (11), we can get $B = S^{(t)}$ and $C = I_d$, where I_d is the identity matrix.

2) LFDA ALGORITHM

Suppose $S^{(lb)}$ is the local between-class scatter matrix and $S^{(lw)}$ is the local within-class scatter matrix:

$$S^{(lb)} := \frac{1}{2}\sum_{i,j=1}^{n'} W_{i,j}^{(lb)}(x_i - x_j)(x_i - x_j)^{\mathrm{T}} \tag{14}$$

$$S^{(lw)} := \frac{1}{2}\sum_{i,j=1}^{n'} W_{i,j}^{(lw)}(x_i - x_j)(x_i - x_j)^{\mathrm{T}} \tag{15}$$

where $W^{(lb)}$ and $W^{(lw)}$ are $n' \times n'$ matrices defined as:

$$W_{i,j}^{(lb)} := \begin{cases} A_{i,j}(1/n' - 1/n'_{y_i}) & \text{if } y_i = y_j \\ 1/n' & \text{if } y_i \neq y_j \end{cases} \tag{16}$$

$$W_{i,j}^{(w)} := \begin{cases} A_{i,j}/n'_{y_i} & \text{if } y_i = y \\ 0 & \text{if } y_i \neq y_j \end{cases} \tag{17}$$

where n'_{y_i} represents the number of labelled samples in its class $y_i \in \{1, 2, \ldots, c\}$, n' is the number of all the labeled samples, $A_{i,j} = \exp(-\frac{\|x_i - x_j\|^2}{\sigma_i\sigma_j})$ is the affinity value between x_i and x_j based on the local scaling heuristic. The parameter $\sigma_i := \|x_i - x_i^k\|$ is a local scaling around x_i.

The transformation matrix in LFDA, $T^{(\mathrm{LFDA})}$, is:

$$T^{(\mathrm{LFDA})} := \arg\max_{T\in R^{d\times r}}[\mathrm{tr}(T^{\mathrm{T}}S^{(lb)}T(T^{\mathrm{T}}S^{(lw)}T)^{-1})] \tag{18}$$

Compared with (11), one can get $B = S^{(lb)}$ and $C = S^{(lw)}$.

TABLE 1. Main parameters of tested engine.

Items	Parameters
Displacement	1.5L
Stroke/ Bore	84.7 mm / 75 mm
Rated power	110 kW @ 5600 r/min
Rated torque	210 Nm @ 2200 r/min -4500 r/min

TABLE 2. Test instruments.

Instrument	Model	Manufacturer
Data collector	SCM05	LMS
Vibration sensor	621B40	IMI SENSORS
Laptop computer	Thinkpad T530	Lenovo
Cylinder pressure sensor	GH13Z-31(24)	AVL

3) SELF ALGORITHM

Suppose $S^{(\mathrm{rlb})}$ is a regularized local between-class scatter matrix and $S^{(\mathrm{rlw})}$ is a regularized local within-class scatter matrix:

$$S^{(\mathrm{rlb})} := (1-\beta)S^{(\mathrm{lb})} + \beta S^{(\mathrm{t})} \tag{19}$$

$$S^{(\mathrm{rlw})} := (1-\beta)S^{(\mathrm{lw})} + \beta I_d \tag{20}$$

where $\beta \in [0, 1]$ is a trade-off parameter. SELF will become LFDA when $\beta = 0$ and PCA when $\beta = 1$.

The transformation matrix in SELF, $T^{(\mathrm{SELF})}$, is:

$$T^{(\mathrm{SELF})} := \underset{T \in R^{d\times r}}{\arg\max}[\mathrm{tr}(T^{\mathrm{T}} S^{(rlb)} T (T^{\mathrm{T}} S^{(rlw)} T)^{-1})] \tag{21}$$

which also can be given as:

$$T^{(\mathrm{SELF})} = (\sqrt{\gamma_1}\varphi_1 \,|\sqrt{\gamma_2}\varphi_2\,|\cdots\,|\sqrt{\gamma_r}\varphi_r) \tag{22}$$

where γ and φ are the eigenvalues and eigenvectors respectively in generalized eigenvalue problem $S^{(\mathrm{rlb})}\varphi = \gamma S^{(\mathrm{rlw})}\varphi$.

III. ENGINE BENCH TEST

The experiment was performed on a turbo charged in-cylinder direct-injection four-cylinder gasoline engine. Engine parameters are listed in Table 1 and the instruments are given in Table 2.

During bench test, vibration signals of engine were collected near the 2nd, 3rd and 4th cylinders by accelerometers. A speed sensor was placed at flywheel end to record the rotatory speed of crankshaft in order to locate top dead center. Every cylinder has a pressure sensor to measure the cylinder pressure for subsequent analysis. A microphone was used to collect the engine knock noise.

The test bench is shown in Fig. 1. The sampling rate was set as 51.2 kHz to cover the knock frequency. The data were collected every 400 r/min from 1200 r/min to 5600 r/min and the testing torque was from 40Nm to 205Nm. Two additional cases of 1400 r/min and 1500 r/min were tested because the engine is prone to knock in this speed range. The level of knock was controlled by adjusting the ignition timing with 2° CA step. The normal working condition is that no knock happens with increasing timing advance until torque drops.

FIGURE 1. Bench test. (a) Engine. (b) Vibration sensors. (c) Cylinder pressure sensors. (d) Testing system.

IV. OPTIMIZATION OF VMD

An optimal VMD proposed based on recursive model (hereafter called RVMD) in [28] is given as follows:

① Calculate the power spectral density (PSD) of input signal f and find the peak frequency, ω_{ini}.

② Set decomposition level K as 1 and take ω_{ini} as the iterative initial center frequency.

③ Take the only one IMF as the first mode u_1.

④ Take $f_2 = f - u_1$ as a new input signal and repeat steps ① -③ to obtain $u_1, u_2, \cdots$.

⑤ Suppose the energy of the kth input signal f_k is E_{tot}, and the energy summation of the kth mode u_k and $f_k - u_k$ is E_x. According to orthogonality, energy difference $E_{err} = E_x - E_{tot}$ is taken as the stop condition for RVMD. The core is that: let the energy of the original input signal f be E_f, $\frac{E_{err}}{E_f} < R_{threshold}$ can be met by looping steps ①-④.

Despite a lot of tests, desired results can be obtained when $R_{threshold} = 0.007$ [28]. However, quadratic penalty α controls the noise in every mode, which has great influence on the energy of signal. That is to say the quadratic penalty α also has considerable effect on the stop condition $R_{threshold}$. So relationship between α and $R_{threshold}$ is explored to improve the RVMD.

In particular, there is generally a most suitable α corresponding to decomposition level K in original VMD. The RVMD has a fixed K value (i.e. K =1), so a fixed α can be selected for it. However, it's difficult to select a suitable α for RVMD, and this paper will do some signals analysis and polynomial fitting in following content to solve this problem.

A. VERIFICATION WITH SIMULATED SIGNAL

For verification, RVMD and EMD are employed to decompose the following simulated signal, as shown in Fig. 2.

$$\begin{cases} s_1 = \begin{cases} 200e^{(-1000*t)}\sin(2\pi f_1 t) & \text{if } t \in [0.0043, 0.0058] \\ 0 & \text{else} \end{cases} \\ s_2 = 30\sin(2\pi f_2 t) \\ s_3 = 50\sin(2\pi f_3 t) \\ s_4 = \eta \\ s = s_1 + s_2 + s_3 + s_4 \end{cases} \tag{23}$$

where $t \in [0, 0.01]$. s_1 ($f_1 = 15000$) simulates attenuated high frequency oscillation signal similar to knock component. s_2 ($f_2 = 2000$) is a high frequency sinusoidal signal. s_3 ($f_3 = 8000$) is low frequency sinusoidal signal. s_4 is 15 dBw Gauss white noise.

Seven IMFs are obtained by EMD but last three of them are obviously illusive components, so only the first four IMFs and the corresponding PSDs are shown in Fig. 3. For the RVMD ($\alpha = 2000$), only 3 IMFs are obtained, are shown in Fig. 4.

As shown in Fig. 3, IMF1 indicates that EMD cannot separate attenuated high frequency oscillation signal (s_1) and the high frequency sine signal (s_2). IMF3 and IMF4 show illusive components in the decomposition. As shown in Fig. 4,

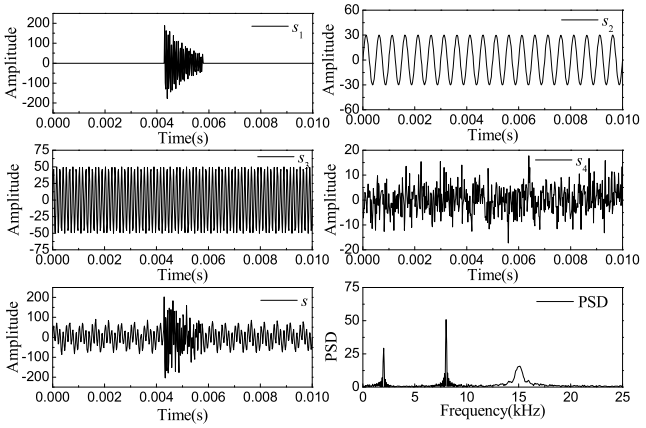

FIGURE 2. Simulated signal.

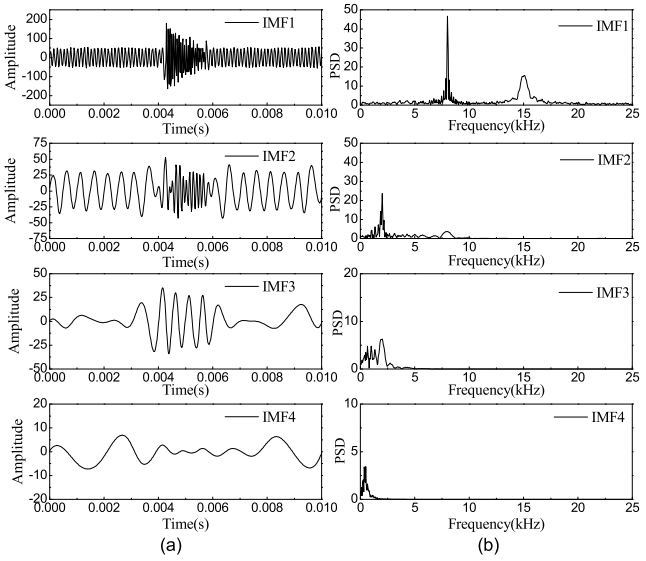

FIGURE 3. Results of EMD. (a) Time domain. (b) Frequency domain.

TABLE 3. Correlation coefficient between decomposition and original components.

Source components		s_1	s_2	s_3
EMD	IMF1	6.67×10^{-1}	6.17×10^{-3}	7.12×10^{-1}
	IMF2	1.18×10^{-2}	7.57×10^{-1}	1.19×10^{-1}
RVMD	IMF1	3.89×10^{-2}	2.14×10^{-2}	$\mathbf{9.92\times10^{-1}}$
	IMF2	1.07×10^{-2}	$\mathbf{9.90\times10^{-1}}$	4.54×10^{-3}
	IMF3	$\mathbf{9.62\times10^{-1}}$	1.72×10^{-4}	8.96×10^{-4}

RVMD can decompose the three original components exactly with desired narrow bandwidth.

To explain the advantages of RVMD quantitatively, the correlation coefficient between decomposition results and original components is calculated and listed in Table 3. The significant difference in correlation coefficient between IMFs and the corresponding original components further illustrates the advantage of RVMD.

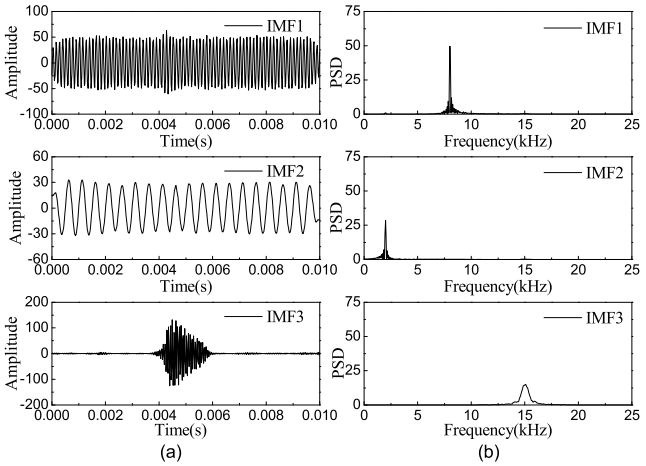

FIGURE 4. Results of RVMD. (a) Time domain. (b) Frequency domain.

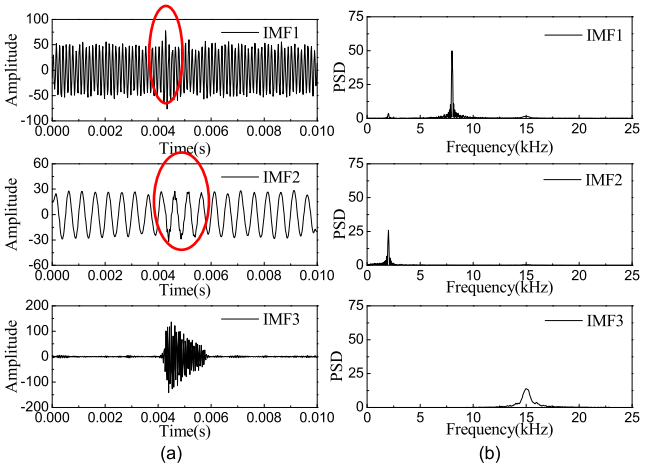

FIGURE 5. Results of a = 500. (a) Time domain. (b) Frequency domain.

B. ANALYSIS OF QUADRATIC PENALTY

To analyze the relationship between the quadratic penalty and the stop condition, $\alpha = 500$ and $\alpha = 10000$ are used to compare with the case of $\alpha = 2000$ (Fig. 4). The $\alpha = 2000$ is default parameter in VMD, and the values 500 and 10000, which are far from 2000, are selected to show and analyze the great influence of α on decomposing results.

As shown in Fig. 5 and Fig. 6, there are large errors in two sinusoidal signals. For smaller α, overlaps with the attenuated high frequency oscillation signal can be found. For larger α, extra component is introduced, which means over-decomposition occurs.

It can be concluded that, the smaller the α is, the higher the noise in signal will be, and vice versa. It is why a small α leads more noise and complex components. On the other hand, it is easier to punish noise excessively when the α is lager and decompose a wide band component into several extra modes. There should be an optimal α value to avoid high noise and over-decomposition at the same time. This is a guarantee of decomposition accuracy of vibration signals and the following recognition rate of knock detection.

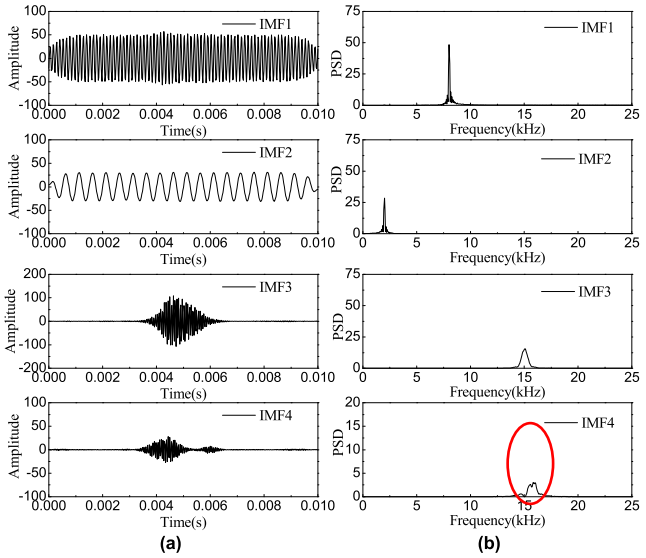

FIGURE 6. Results of a = 10000. (a) Time domain. (b) Frequency domain.

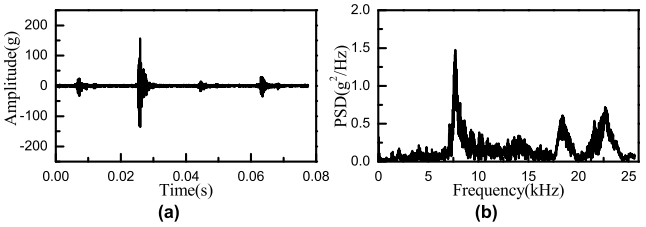

FIGURE 7. Measured vibration signal. (a) Time domain. (b) Frequency domain.

C. OPTIMIZATION OF QUADRATIC PENALTY

In this section, a real vibration signal, measured from the 3rd cylinder at 1600 r/min speed with 85 Nm torque and 8.25 °CA timing advance increment, is used to investigate the relationship between quadratic penalty α and stop condition $R_{threshold}$.

The time history and frequency spectrum of the signal is shown in Fig. 7. The firing order is 4-2-1-3. Based on the cylinder pressure, the 2nd cylinder is found under strong knock condition, the 3rd cylinder is under slight knock condition, and the 1st and 4th cylinder are in normal working condition.

As mentioned above, it is supposed the ratio of the energy difference at desired stop condition ($E_{err-threshold}$) to original signal's energy (E_f) is $R_{threshold}$ and ratio of the energy difference when iteration stopping (E_{err-k}) to E_f is R_k. Let $R_{nor} = R_k/R_{threshold}$, and R_{nor} will be used to investigate the influence of quadratic penalty α. R_k must be less than $R_{threshold}$ so that $R_{nor} < 1$, which means R_{nor} can express the relationship between quadratic penalty and results clearly.

In processing the measured vibration signal, the stop condition $R_{threshold}$ increases from 0.005 to 0.020 by 0.001 and the quadratic penalty α increases from 1000 to 10000 by 100.The results of R_{nor} is shown as Fig. 8.

When signals are decomposed with RVMD, it is desirable that R_{nor} can be stable and close to 1. The stability can

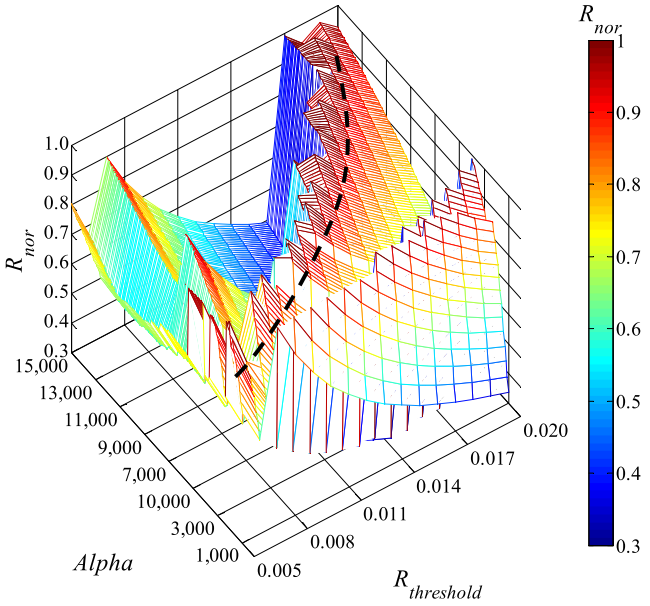

FIGURE 8. Results of R_{nor} in different conditions.

TABLE 4. RMSEs of fitting formulas.

Order	RMSE
1st	9.97×10^{-2}
2nd	8.53×10^{-2}
3rd	6.98×10^{-2}
4th	6.98×10^{-2}
5th	6.66×10^{-2}
6th	6.66×10^{-2}

provide good consistency of decomposition, and the value close to 1 means it's no need to punish noise by α and $R_{threshold}$ excessively. Under these considerations, $R_{nor} = 0.80 - 0.90$ is appropriate. A required continuous area exists in Fig 8 as marked with black dashed line. In this area, the α and $R_{threshold}$ are corresponding to each other and can be shown in two-dimensional coordinate system. All of these points are extracted and shown in Fig. 9.

As shown in Fig. 9, the relationship between α and $R_{threshold}$ can be expressed by curve fitting. Because of the great magnitude difference between α and $R_{threshold}$, they are fitted by their natural logarithms. To find the best fitting formula, Root Mean Square Error (RMSE) is used.

$$RMSE = \sqrt{\frac{1}{n}\sum_{i=1}^{n}(y_i - \hat{y}_i)^2} \tag{24}$$

where n is the number of samples, y_i is the original value and $\hat{y}_i$ is the fitted value.

In this paper, 1st-6th polynomial fittings are calculated and the RMSEs are listed in Table 4.

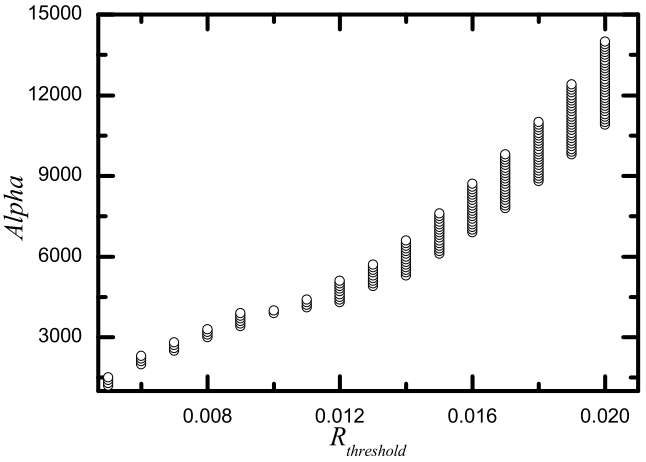

FIGURE 9. Scatter plot of required points.

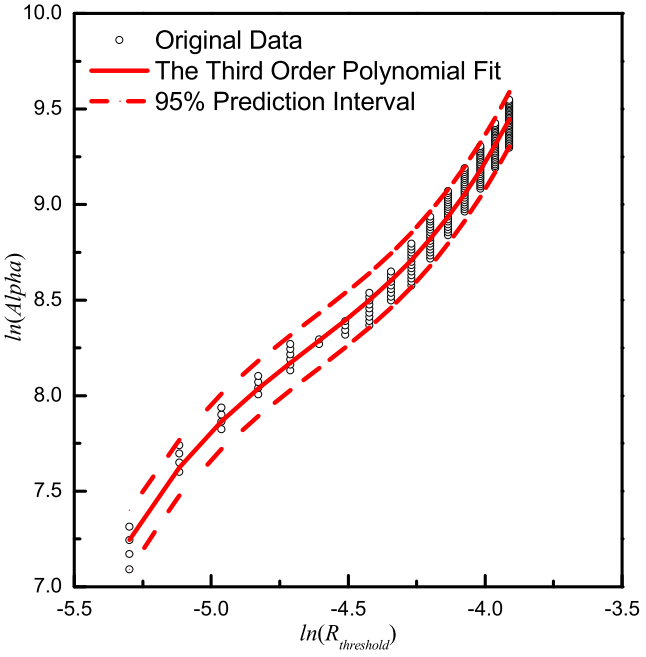

FIGURE 10. Results of 3rd polynomial fit.

As shown in Table 4, the RMSE does not decline obviously with increasing order higher than 3. However, with the increasing of order, the complexity increases obviously. Upon comprehensive consideration, the 3rd polynomial is reasonable choice and the 3rd fitting result is shown as Fig. 10.

The fitting formula is:

$$\begin{aligned}\ln(\alpha) = {} & 1.015[\ln(R_{threshold})]^3 + 14.154[\ln(R_{threshold})]^2 \\ & +66.838\ln(R_{threshold}) + 115.121\end{aligned} \tag{25}$$

That is:

$$\begin{aligned}\alpha = {} & e^{1}.015[\ln(R_{threshold})]^3 \\ & +14.154[\ln(R_{threshold})]^2 \\ & +66.838\ln(R_{threshold}) + 115.121\end{aligned} \tag{26}$$

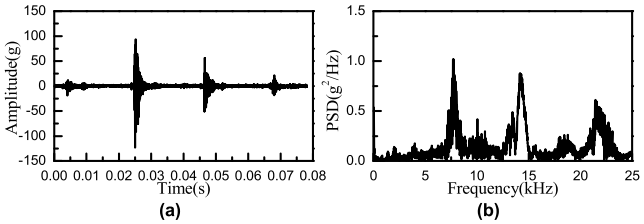

FIGURE 11. Verification signal. (a) Time domain. (b) Frequency domain.

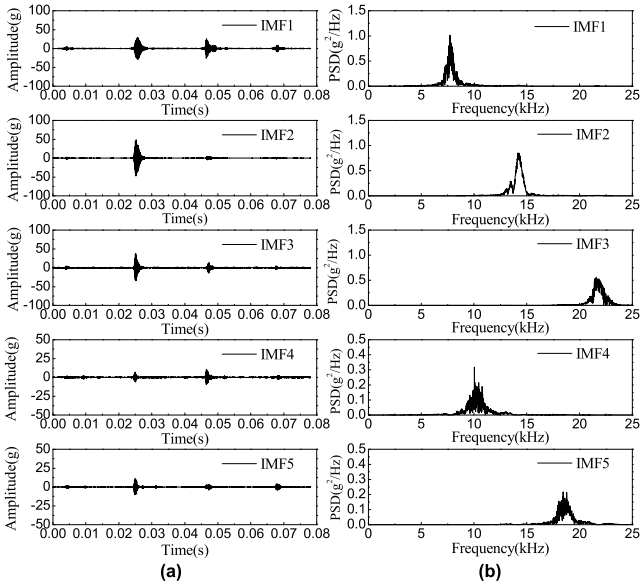

FIGURE 12. Result the of a = 2860. (a) Time domain. (b) Frequency domain.

To verify the accuracy and adaptability of fitting formula (26), another measured signal is used, which is collected under 1400 r/min with timing advance increment of 6.00 °CA as shown in Fig. 11. When decomposing knock signals by RVMD, α is calculated by fitting formula (26) as 2860 in the case of $R_{threshold} = 0.007$, and the result is shown as Fig. 12.

As shown in Fig. 12, the fitted α give desired result by extracting every component exactly without under-decomposition and over-decomposition. The result proves that the fitting formula proposed has ability to choose appropriate α for RVMD. This work can insure the accuracy of decomposition and guarantee to recognize knock in different intensities.

V. MULTILEVEL SELF ALGORITHM

In consideration of knock characteristic frequency, the components in 5 kHz-20 kHz will be restructured. After decomposition and restructuration, knock intensity can be recognized by calculating characteristic parameters.

Single kind of characteristic parameter can hardly characterize knock due to lack of information. So standard deviation, skewness, kurtosis, peak to peak, square root amplitude, average amplitude, RMS, Shannon entropy, the largest singular value and fourth-order cumulant are

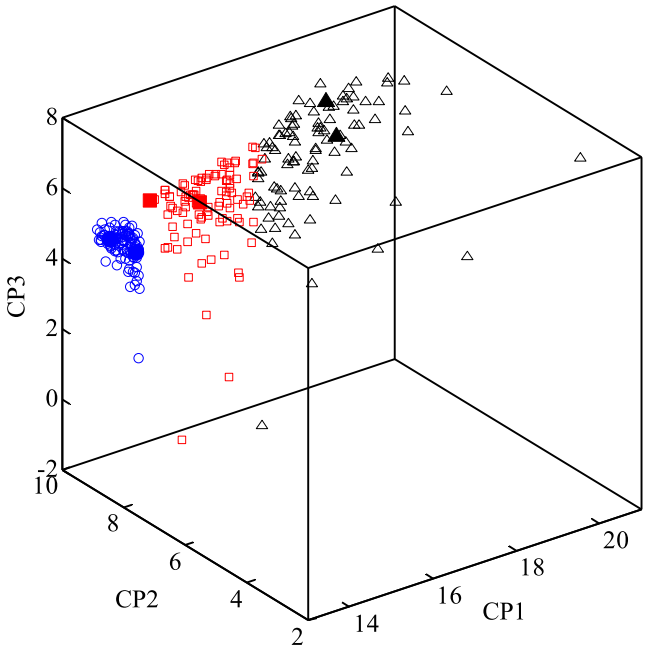

FIGURE 13. 3-dimensional samples of 1-level dimensionality reduction, where the blue "●" represents labeled samples of normal condition, the blue "○" represents unlabeled samples of normal condition, the red "■" represents labeled samples of slight knock, the red "□" represents unlabeled samples of slight knock, the black "▲" represents labeled samples of strong knock, the black "△" represents unlabeled samples of strong knock.

calculated. Their calculation principles and physical significances are shown in Appendix.

Specially, the advantages of SELF have been proved in [24] and it is not shown in this paper for limited space. The multilevel SELF proposed in this paper will be expressed in detail as follows.

102 data sets of normal condition, slight knock condition and strong knock condition signals are selected respectively according to maximum amplitude of pressure oscillation (MAPO). For each condition, 2 sets of signals are selected randomly as labeled samples and the rest 100 sets of each condition are taken as unlabeled samples to calculate recognition rate.

A. SELF ANALYSIS

To describe multilevel SELF algorithm clearly, a brief analysis and an example are shown in this section. The trade-off parameter β is selected as 0.5. The 10-dimensional samples are reduced to 3-dimensional ones by SELF directly (see Fig. 13) and the results are shown in their natural logarithms because of great scale difference. The low-dimension characteristic parameters are named as CP.

As shown in Fig. 13, there are several embedded spaces can transform 3-dimensional samples into 2-dimensional ones. Fig. 14 shows the 2-dimensional samples transformed by SELF directly from original 10-dimensional ones. In Fig. 14, the 2-dimensional samples can be understood as reducing dimensionality from those in Fig. 13 by the embedded space composed of CP1 vector and CP2 vector approximately.

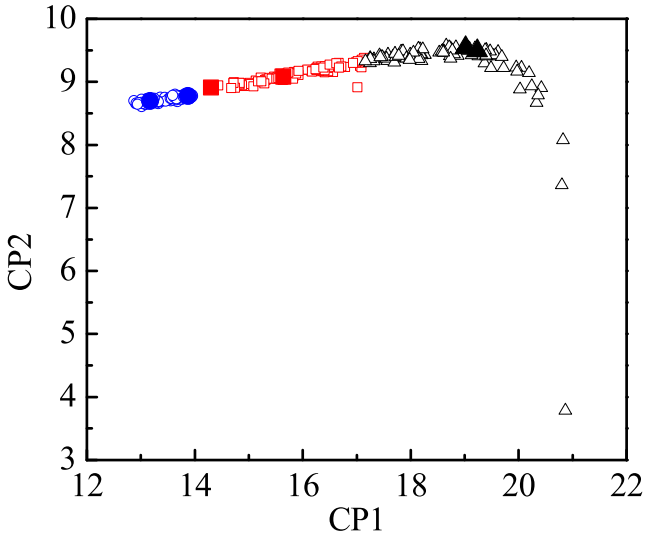

FIGURE 14. 2-dimensional samples of 1-level dimensionality reduction, where the blue "●" represents labeled samples of normal condition, the blue "○" represents unlabeled samples of normal condition, the red "■" represents labeled samples of slight knock, the red "□" represents unlabeled samples of slight knock, the black "▲" represents labeled samples of strong knock, the black "△" represents unlabeled samples of strong knock.

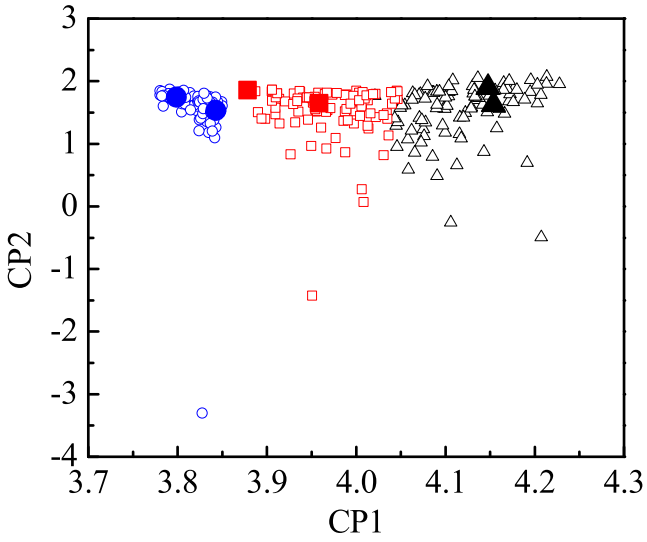

FIGURE 15. 2-dimensional samples of 2-level dimensionality reduction, where the blue "●" represents labeled samples of normal condition, the blue "○" represents unlabeled samples of normal condition, the red "■" represents labeled samples of slight knock, the red "□" represents unlabeled samples of slight knock, the black "▲" represents labeled samples of strong knock, the black "△" represents unlabeled samples of strong knock.

To investigate other embedded spaces, it is tried to process original samples by 2-level dimensionality reduction which the first level is 3 dimensions and the second level is 2 dimensions. That is reducing the 10-dimensional original samples to 3-dimensional ones, and then reducing the 3-dimensional samples to 2-dimensional ones. The 2-dimensional samples are taken as final results, and are shown as Fig. 15.

As shown in Fig. 15, different structures can be found after 2-level dimensionality reduction. When the dimension reduced is high, SELF sometimes may not find the best transformation matrix. That means a multilevel dimensionality reduction may have better chance to find the best low-dimensional space by several transformation matrixes with descending dimensions. Based on that, multilevel SELF algorithm can be proposed.

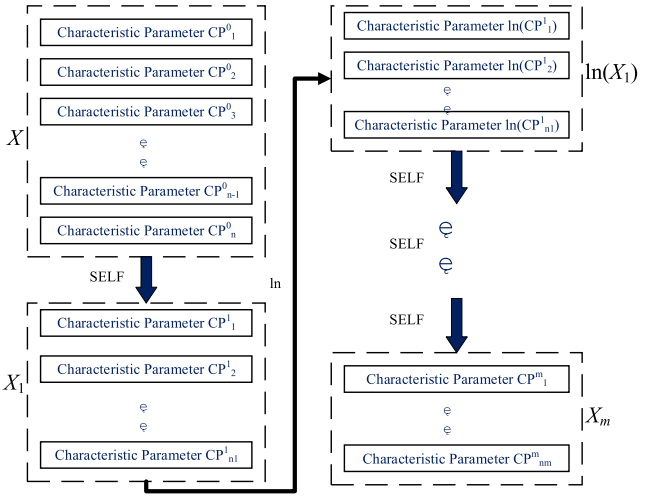

FIGURE 16. Workflow of SELF algorithm, where *m* is the level of multilevel SELF, and *n* is the dimensionality of samples.

B. MULTILEVEL SELF ALGORITHM

The process of multilevel SELF algorithm is given as follows:

① For n-dimensional data X, reduce its dimensionality to n_1-dimensional by SELF and obtain low dimension data X_1, where $n_1 < n$, and n_1 is a positive integer.

② Let the natural logarithm of X_1 as $\ln(X_1)$, and take $\ln(X_1)$ as input for subsequent computations.

③ Reduce the dimensionality of $\ln(X_1)$ to n_2 by SELF and obtain the result X_2, where $n_2 < n_1$, and n_2 is a positive integer.

④ With reasonable structural design, several descending n values are selected, $n_2 > n_3 > \cdots > n_m$, to repeat step ③ until the final result X_m with n_m-dimensional is obtained.

Specifically, the $n_2 > n_3 > \cdots > n_m$ are not continue positive integers instead of abrupt change ones. Only X_1 is calculated its natural logarithm.

The workflow of multilevel SELF algorithm is shown in Fig. 16.

C. STRUCTURE AND VERIFICATION OF MULTILEVEL SELF ALGORITHM

More accurate results can be obtained by multilevel SELF structure, but the efficiency reduces when structure becomes more complex. With a lot of testing and adjusting, the structure of 5-3-1 shows the best performance. The dimensionality reduction result of original data is shown as Fig. 17.

As shown in Fig. 17, different working conditions can be clearly observed from the result of multilevel SELF. In order to analyze the accuracy quantitatively, an unsupervised classifier fuzzy c-means clustering (FCM) is introduced to

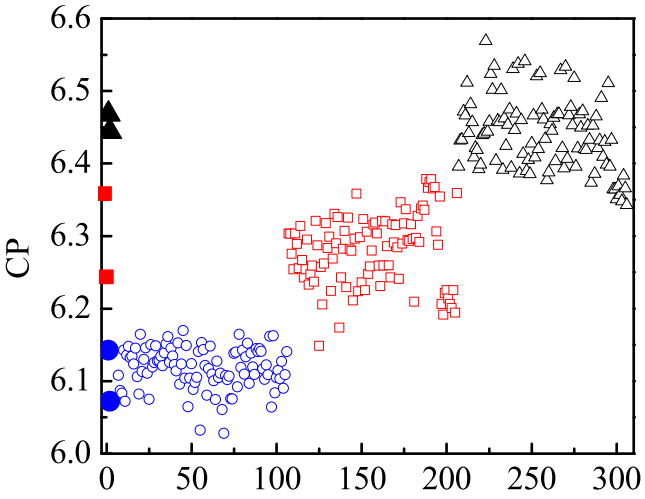

FIGURE 17. Result of multilevel SELF, where the blue "●" represents labeled samples of normal condition, the blue "○" represents unlabeled samples of normal condition, the red "■" represents labeled samples of slight knock, the red "□" represents unlabeled samples of slight knock, the black "▲" represents labeled samples of strong knock, the black "△" represents unlabeled samples of strong knock.

TABLE 5. Classification rate of multilevel SELF with 5-3-1 structure.

Working condition	Normal condition	Slight knock	Strong knock
Classification rate	92.59%	91.75%	96.84%

evaluate the distinguishability of the results. FCM is a classical classifier, the reason for selecting it is that the FCM has high efficiency and does not need training by labeled samples. These advantages accord with the demands of using as few as possible labeled samples to detect knock quickly.

For clear comparison, the classification rate is defined as: Classification Rate $= \frac{\text{data}_r}{\text{data}_a}$, where data_a is the number of samples recognized in a certain class by FCM, where $\text{data}_a = \begin{cases} \text{data}_a & \text{if } \text{data}_a \geq 100 \\ 100 & \text{if } \text{data}_a < 100 \end{cases}$, and data_r is the number of samples recognized correctly in this certain class.

As shown in Table 5, the result of the multilevel SELF with 5-3-1 structure shows high accuracy in knock detection. All classification rates are over 90%, and the classification rate of strong knock is over 95%.

To verify the effectiveness and practicability of multilevel SELF, original SELF and several multilevel SELF algorithms with different structures are used to process the samples. In Table 6, the structure with only one level is the original SELF, and the number of structure (such as 3-1) represents the reduced dimensionality in each level.

As shown in Table 6, the original SELF algorithms, such as structures "3", "2", and "1", have generally lower accuracy compared with multilevel SELF algorithms. The multilevel SELF with simple structure "3-1" is more accurate than the original SELF. For structure "9-7-5-3-2-1" and "9-8-7-6-5-4-3-2-1", their accuracies are the same as the proposed structure "5-3-1", but they are less efficient.

TABLE 6. Classification rate of SELF with different structures.

Working condition		Normal condition	Slight knock	Strong knock
The algorithm structure	3	86.21%	77.06%	75.00%
	2	87.72%	85.15%	85.00%
	1	87.72%	82.69%	82.00%
	3-1	91.74%	88.35%	88.00%
	9-7-5-3-2-1	92.59%	91.75%	96.84%
	9-8-7-6-5-4-3-2-1	92.59%	91.75%	96.84%

TABLE 7. Classification rate of single characteristic parameter.

Working condition	Normal condition	Slight knock	Strong knock
Standard deviation	67.11%	50.00%	49.00%
Skewness	47.83%	44.23%	70.73%
Kurtosis	58.48%	27.27%	19.00%
Peak to peak	59.17%	35.23%	43.00%
Square root amplitude	86.21%	65.63%	56.00%
Average amplitude	79.37%	61.16%	53.00%
RMS	67.11%	50.00%	49.00%
Shannon entropy	59.78%	35.66%	56.96%
The largest singular value	67.11%	50.00%	49.00%
Fourth-order cumulant	38.61%	0.00%	33.00%
All the ten parameters	38.76%	0.00%	8.00%

To verify the necessity of SELF, classification rate of knock detection for every single characteristic parameter is also evaluated. The results are shown as Table 7.

As shown in Table 7, using single characteristic parameter cannot recognize different intensities of knock accurately. In opposite, using all the ten original characteristic parameters is not able to well detect knocks either.

VI. CONCLUSION AND DISCUSSION

A. CONCLUSION

In order to detect engine knock in different intensities, a novel approach is proposed:

1) A 3rd order polynomial fitting function is developed to reduce the subjectivity of quadratic penalty α in RVMD based on analyzing the relationship between quadratic penalty α and energy difference stop condition.
2) A multilevel SELF composed of several embedding spaces with decreasing dimensions is proposed, which can reduce the dimensionality of original samples gradually.
3) In application, vibration signals are decomposed by RVMD and then knock characteristics are restructured. Ten characteristic parameters of the reconstructed

signal are calculated. High-dimensional samples are processed by multilevel SELF and recognized by FCM. A "5-3-1" multilevel SELF is found of best knock recognition performance.

The method proposed in this paper can recognize knock in different intensities accurately and has certain theory and engineering practice significances.

B. DISCUSSION AND OUTLOOK

There is also more work worth further research:

1) In term of the fitting function of quadratic penalty for RVMD, extra points can also get desired results. The objective of this paper is to find a concise method to describe the relationship between quadratic penalty α and energy difference stop condition, which makes it possible that values within the margin can get same results. In future work, the determination of exact α value can be explored depending on the investigation of signals' physical significance.
2) For multilevel SELF, the classifier is chosen as FCM because its efficiency and conciseness for labeled samples. However, FCM is traditional and simple, and more advanced classifiers will be studied in the succeeding work.

APPENDIX
THE CALCULATION PRINCIPLES AND PHYSICAL SIGNIFICANCES OF CHARACTERISTIC PARAMETERS

Suppose $X = [x_1, x_1, \ldots x_n]$ is a set of random variable, so:

1) STANDARD DEVIATION

$$S = \sqrt{\frac{1}{n-1}\sum_{i=1}^{n}|x_i - \bar{x}|^2}$$

where $\bar{x} = \frac{1}{n}\sum_{i=1}^{n} x_i$, i.e. the mean of X.

The standard deviation can describe the dispersion of data and can be understood as impact strength.

2) SKEWNESS

$$sk = \frac{\frac{1}{n}\sum_{i=1}^{n}(x_i - \bar{x})^3}{S^3}$$

The skewness can describe the lopsidedness of data and can be understood as directional tendency.

3) KURTOSIS

$$k = \frac{\frac{1}{n}\sum_{i=1}^{n}(x_i - \bar{x})^4}{S^4}$$

The kurtosis can describe the degree of deviation from normal distribution and can be understood as the abnormity degree of data.

4) PEAK TO PEAK

$$p - p = |max\,(X) - min\,(X)|$$

The peak to peak is the difference between the minimum and maximum values, and can be understood as the biggest change in data.

5) SQUARE ROOT AMPLITUDE

$$sra = \left(\frac{1}{n}\sum_{i=1}^{n}\sqrt{|x_i|}\right)^2$$

The square root amplitude is part of margin index and can describe the signal-to-noise ratio.

6) AVERAGE AMPLITUDE

$$|X| = \frac{1}{n}\sum_{i=1}^{n}|x_i|$$

The average amplitude is the measurement for overall amplitude of data.

7) ROOT MEAN SQUARE (RMS)

$$RMS = \sqrt{\sum_{i=1}^{n} x_i^2}$$

The RMS can be understood as the effective value of data.

8) SHANNON ENTROPY

Suppose the chance of x_i exists in X is p_i, and $\sum_{i=1}^{n} p_i = 1$. So the Shannon Entropy of X is: $Sha = \sum_{i=1}^{n} p_i \ln p_i$.

The Shannon Entropy can describe uncertainty of data.

9) THE LARGEST SINGULAR VALUE

Suppose A is a $m \times n$ matrix, and there must be orthogonal (or unitary) matrix $U^T U = I_m$ and $V^T V = I_n$ let $A_{m\times n} = U_{m\times n}\Sigma_{m\times n}V^T_{m\times n}$, where the $\sum$ is orthogonal matrix, which $\sum = diag(\lambda_1, \lambda_2, \ldots \lambda_r)$ and rank(A) = rank$(\sum) = r$. The diagonal elements of $\sum$ is the singular values of A and the largest singular value is the largest of them.

The largest singular value can be understood as the maximum growth rate of disturbance in a certain period of time.

10) FOURTH-ORDER CUMULANT

Suppose the probability density function of X is $f(x)$, and then the first eigenfunction of X is:

$$\Phi(\omega) = E\{e^{j\omega x}\} = \int_{-\infty}^{\infty} f(x)e^{j\omega x}dx$$

The kth derivative of it is:

$$\Phi^k(\omega) = \frac{d^k\Phi(\omega)}{d\omega^k} = j^k E\{x^k e^{j\omega x}\}$$

Let $\omega = 0$, the kth order moment of X is:

$$m_k = \Phi^k(0) = E\{x^k\}$$

Let $\Psi(\omega) = \ln \Phi(\omega)$, so the kth order cumulant of X is defined as the value of the kth derivative of $\Psi(\omega)$ at $\omega = 0$:

$$c_k = \frac{d^k \Psi(\omega)}{d\omega^k} |_{\omega=0}$$

The fourth-order cumulant can be understood as the degree of deviation from Gaussian noise.

REFERENCES

[1] A. Boretti, "Towards 40% efficiency with BMEP exceeding 30 bar in directly injected, turbocharged, spark ignition ethanol engines," *Energy Convers. Manage.*, vol. 57, pp. 154–166, May 2012.
[2] Z. Wang, H. Liu, and R. D. Reitz, "Knocking combustion in spark-ignition engines," *Prog. Energy Combust. Sci.*, vol. 61, pp. 78–112, Jul. 2017.
[3] M. S. Lounici, M. A. Benbellil, K. Loubar, D. C. Niculescu, and M. Tazerout, "Knock characterization and development of a new knock indicator for dual-fuel engines," *Energy*, vol. 141, pp. 2351–2361, Dec. 2017.
[4] D.-U. Yun and S.-K. Lee, "Objective evaluation of the knocking sound of a diesel engine considering the temporal and frequency masking effect simultaneously," *J. Sound Vibrat.*, vol. 397, pp. 282–297, Jun. 2017.
[5] X. Zhen, Y. Wang, S. Xu, Y. Zhu, C. Tao, T. Xu, and M. Song, "The engine knock analysis—An overview," *Appl. Energy*, vol. 92, pp. 628–636, Apr. 2012.
[6] Z.-Y. Wu, H.-Q. Yuan, and S. Li, "Fault diagnosis based on EMD and fuzzy clustering for diesel engine," *J. Northeastern Univ. Natural Sci.*, vol. 30, no. 12, pp. 1784–1787, 2009.
[7] Y.-P. Cai, A.-H. Li, L.-S. Shi, P. Xu, and W. Zhang, "IC engine fault diagnosis method based on EMD-WVD vibration spectrum time-frequency image recognition by SVM," *Chin. Internal Combustion Engine Eng.*, vol. 33, no. 2, pp. 72–78, 2012.
[8] A. Moreno-Gomez, J. P. Amezquita-Sanchez, M. Valtierra-Rodriguez, C. A. Perez-Ramirez, A. Dominguez-Gonzalez, and O. Chavez-Alegria, "EMD-Shannon entropy-based methodology to detect incipient damages in a truss structure," *Appl. Sci.*, vol. 8, no. 11, p. 2068, Oct. 2018.
[9] A. Sharma, V. Sugumaran, and S. B. Devasenapati, "Misfire detection in an IC engine using vibration signal and decision tree algorithms," *Measurement*, vol. 50, pp. 370–380, Apr. 2014.
[10] A. Taghizadeh-Alisaraei, B. Ghobadian, T. Tavakoli-Hashjin, S. S. Mohtasebi, A. Rezaei-asl, and M. Azadbakht, "Characterization of engine's combustion-vibration using diesel and biodiesel fuel blends by time-frequency methods: A case study," *Renew. Energy*, vol. 95, pp. 422–432, Sep. 2016.
[11] S. K. Yadav and P. K. Kalra, "Fault diagnosis of internal combustion engine using empirical mode decomposition," in *Proc. 6th Int. Symp. Image Signal Process. Anal.*, Sep. 2009, pp. 40–46.
[12] N. E. Huang, Z. Shen, S. R. Long, M. C. Wu, H. H. Shih, Q. Zheng, N. C. Yen, C. C. Tung, and H. H. Liu, "The empirical mode decomposition and the Hilbert spectrum for nonlinear and non-stationary time series analysis," *Proc. Roy. Soc. London Ser. A, Math., Phys. Eng. Sci.*, vol. 454, no. 1971, pp. 903–995, Mar. 1998.
[13] B. Chen, Z. He, X. Chen, H. Cao, G. Cai, and Y. Zi, "A demodulating approach based on local mean decomposition and its applications in mechanical fault diagnosis," *Meas. Sci. Technol.*, vol. 22, no. 5, May 2011. Art. no. 055704.
[14] J. Zheng, J. Cheng, and Y. Yang, "A rolling bearing fault diagnosis approach based on LCD and fuzzy entropy," *Mechanism Mach. Theory*, vol. 70, pp. 441–453, Dec. 2013.
[15] J.-R. Yeh, J.-S. Shieh, and N. E. Huang, "Complementary ensemble empirical mode decomposition: A novel noise enhanced data analysis method," *Adv. Adapt. Data Anal.*, vol. 2, no. 2, pp. 135–156, Apr. 2010.
[16] X.-M. Xue, J.-Z. Zhou, Y.-H. Xu, W.-L. Zhu, and C.-S. Li, "An adaptively fast ensemble empirical mode decomposition method and its applications to rolling element bearing fault diagnosis," *Mech. Syst. Signal Process.*, vols. 62–63, pp. 444–459, Oct. 2015.
[17] K. Dragomiretskiy and D. Zosso, "Variational mode decomposition," *IEEE Trans. Signal Process.*, vol. 62, no. 3, pp. 531–544, Feb. 2014.
[18] X. Bi, S. Cao, and D. Zhang, "Diesel engine valve clearance fault diagnosis based on improved variational mode decomposition and bispectrum," *Energies*, vol. 12, no. 4, p. 661, Feb. 2019.
[19] X. Bi, S. Cao, and D. Zhang, "A variety of engine faults detection based on optimized variational mode decomposition-robust independent component analysis and fuzzy c-mean clustering," *IEEE Access*, vol. 7, pp. 27756–27768, 2019.
[20] I. Guyon and A. Elisseeff, "An introduction to variable and feature selection," *J. Mach. Learn. Res.*, vol. 3, pp. 1157–1182, Jan. 2003.
[21] R. Kohavi and G. H. John, "Wrappers for feature subset selection," *Artif. Intell.*, vol. 97, nos. 1–2, pp. 273–324, 1997.
[22] X. Yu, F. Dong, E. J. Ding, S. P. Wu, and C. Y. Fan, "Rolling bearing fault diagnosis using modified LFDA and EMD with sensitive feature selection," *IEEE Access*, vol. 6, pp. 3715–3730, 2018.
[23] I. T. Jolliffe, N. T. Trendafilov, and M. Uddin, "A modified principal component technique based on the LASSO," *J. Comput. Graph. Statist.*, vol. 12, no. 3, pp. 531–547, 2003.
[24] M. Sugiyama, T. Idé, S. Nakajima, and J. Sese, "Semi-supervised local Fisher discriminant analysis for dimensionality reduction," *Mach. Learn.*, vol. 78, nos. 1–2, pp. 35–61, Jan. 2010.
[25] Y. Wang, J. Wang, H. Y. Chen, and B. Sun, "Semi-supervised local Fisher discriminant analysis based on reconstruction probability class," *Int. J. Pattern Recognit. Artif. Intell.*, vol. 29, no. 2, Mar. 2015. Art. no. 1550007.
[26] G. Tur, D. Hakkani-Tür, and R. E. Schapire, "Combining active and semi-supervised learning for spoken language understanding," *Speech Commun.*, vol. 45, no. 2, pp. 171–186, Feb. 2005.
[27] H. Huang, J. Li, and J. Liu, "Gene expression data classification based on improved semi-supervised local Fisher discriminant analysis," *Expert Syst. Appl.*, vol. 39, no. 3, pp. 2314–2320, Feb. 2012.
[28] F. Bi, X. Li, C. Liu, C. Tian, T. Ma, and X. Yang, "Knock detection based on the optimized variational mode decomposition," *Measurement*, vol. 140, pp. 1–13, Jul. 2019.

FENGRONG BI received the doctor's degree in power machinery and engineering from Tianjin University, Tianjin, China, in 2003, where he is currently a Professor. He is also the Co-Director of the Engineering Center for Advanced Automotive Technologies, Tianjin University-RMIT. His main research interests include vehicle dynamics, vibration and noise control, reliability, and weak power fault diagnosis.

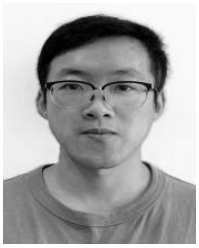

XIN LI received the master's degree in power machinery and engineering from Tianjin University, Tianjin, China, in 2017, where he is currently pursuing the doctor's degree. His main research interests include reliability and weak power fault diagnosis.

JIEWEI LIN received the Ph.D. degree in power machinery and engineering from Tianjin University, China. After a Research Fellow experience in the Institute of Sound and Vibration Research, University of Southampton, U.K., he joined the State Key Laboratory of Engines, Tianjin University, as an Associate Professor. His research interests include noise and vibration control of engine and vehicle.

XIAOBO BI received the master's degree in vehicle engineering from the Hebei University of Technology, Tianjin, China. He is currently pursuing the Ph.D. degree in power machine and engineering with the State Key Laboratory of Engines, Tianjin University, Tianjin. He is currently a Senior Lecturer with the Hebei University of Technology. His research interests include multi-information fusion fault diagnosis of ICE and NVH control of vehicle.

TENG MA received the bachelor's degree in vehicle engineering from the Hebei University of Technology, and the master's degree in power machine and engineering from Tianjin University, where he is currently pursuing the Ph.D. degree in power machine and engineering with the State Key Laboratory of Engines. His research interests include engine knock control and vibration control of vehicle.

XIAO YANG graduated from Tianjin University, Tianjin, China, where he is currently pursuing the Ph.D. degree in power machine and engineering with the State Key Laboratory of Engines. His current research interests include fault diagnosis and noise reduction of internal combustion engines.

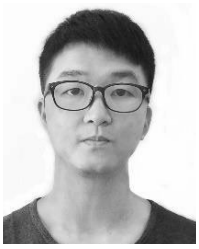

DAIJIE TANG received the B.S. degree in energy and power engineering and the M.S. degree in power engineering from Tianjin University, Tianjin, China, in 2016 and 2019, respectively, where he is currently pursuing the Ph.D. degree in power machinery and engineering. His current research interests include fault diagnosis of power machinery, vibration, and noise control.

PENGFEI SHEN received the B.S. degree from Tianjin University, Tianjin, China, where he is currently pursuing the M.S. degree in powering engineering. His main research interest includes the power machinery's vibration fault diagnosis.